ELSEVIER

Coordination Chemistry Reviews
212 (2001) 11–34

COORDINATION CHEMISTRY REVIEWS

www.elsevier.com/locate/ccr

The ligand field molecular mechanics model and the stereoelectronic effects of d and s electrons

Robert J. Deeth *

Department of Chemistry, Inorganic Computational Chemistry Group, University of Warwick, Coventry CV4 7AL, UK

Received 20 October 1999; accepted 10 March 2000

Contents

* Tel.: +44-247-6523187; fax: +44-247-6524112.
E-mail address: r.j.deeth@warwick.ac.uk (R.J. Deeth).

PII: S0010-8545(00)00354-4

Abstract

This review discusses modifications and extensions of Molecular Mechanics which are designed to model the electronic effects of the valence d and s electrons in transition metal compounds. These effects lead to severe distortions away from the ideal geometries predicted by simple VSEPR theory. The stereochemical activity of d electrons manifests in a range of structural distortions of ionic coordination complexes typified by the Jahn–Teller elongations of six-coordinate d^9 Cu^{2+} species. Modelling these effects requires an additional term in the strain energy which describes the attendant ligand field stabilisation energy (LFSE). The LFSE is explicitly incorporated into the ligand field molecular mechanics (LFMM) method which has been applied to a range of complexes of Cu^{2+}, Ni^{2+} and Co^{3+}. A single set of LFMM parameters for a given metal–ligand interaction is able to model different coordination numbers, spin states and bond lengths. The stereochemical activity of the valence metal s orbital is significant for covalent organometallic species such as WMe_6 which does not show the regular octahedral geometry expected for a formally d^0 system. The effect can be treated within Valence Bond theory by modifying the expressions for the angle bending potentials based on Pauling's strength functions for sd^n hybrids. There is more than one idealised bond angle for sd^3, sd^4 and sd^5 hybrids which correlates with the irregular geometries found for hydride, alkyl and aryl compounds. The same behaviour can also be obtained within the LFMM scheme by using an extended stabilisation energy term which incorporates the s orbital contributions. The LFMM model also predicts the ligand field contribution to the activation energy for ligand exchange/substitution and can be used to calculate the structures and energies of transition states as illustrated by model calculations for the reactions of low-spin d^8 complexes.

Keywords: Molecular modelling; Transition metal complexes; Electronic effects

1. Introduction

Transition metal compounds display a rich diversity of structure. The number of ligands attached to a metal centre may range from one to twelve and, for a given coordination number, multiple geometries are possible depending on the particular combination of ligands, metal, oxidation state and spin state. However, the most common coordination numbers are 4, 5 and 6 and each is associated with an 'ideal' geometry – tetrahedral (tet), trigonal bipyramidal (tbp) and octahedral (oct) respectively. These regular geometries arise naturally from a consideration of, for example, the mutual repulsion between point charges on the surface of a sphere or between the electrons in the M–L bonds and any stereochemically active lone pairs.

Computer modelling of TM systems is booming with much of the activity directed at the application of quantum chemistry, notably Density Functional Theory (DFT) [1,2]. Yet, even though DFT is efficient, at least compared to other ab initio schemes, it can never compete with the speed of empirical Molecular Mechanics. However, the accuracy of MM treatments for TM systems remains problematic.

Regular geometries do not pose significant technical difficulties for conventional Molecular Mechanics (MM) at least from a strictly mathematical point of view. Of course, developing useful and transferable sets of Force Field (FF) parameters capable of dealing with more or less regular tetrahedral, trigonal bipyramidal and octahedral complexes remains a challenging exercise [3]. However, this review focuses on the even more challenging problem of modelling irregular four-, five- and six-coordinate species particularly when valence electronic effects play a significant role in determining the molecular structure [4–7].

Two general classes of distorted structures can be identified. Each is associated with a different mechanism 'driving' the distortion. Class I refers to classical Werner-type coordination complexes with an incomplete shell of d electrons. Distortions from the regular structures described above can be traced to the stereochemical activity of the d-electrons [8] and the attendant Ligand Field Stabilisation Energy (LFSE). The observed structure is thus a balance between the need to maximise the LFSE (i.e. minimise the d electronic energy) whilst minimising the ligand–ligand interactions. Treating this effect within a MM framework requires an extra term in the strain energy expression [6]. This term is based on generalised Ligand Field Theory (LFT) and leads to the Ligand Field–Molecular Mechanics (LFMM) model [6]. Compounds in Class II are covalent organometallic species. Here, deviations from regular geometries can be rationalised by inclusion of s-orbital participation in bonding in the sense that the angular geometry can be predicted on the basis of the disposition of sd^n hybrids arising from Valence Bond (VB) theory [9]. The structures of such compounds can be modelled within MM by modifying the angle-bending term to reflect the ideal bond angles between sd^n hybrid orbitals. Alternatively, the same angular potential around the metal can be captured within the LFMM scheme by incorporating s-orbital contributions directly into the electronic energy calculation.

The division of molecules into Class I and II roughly parallels some formal notions of covalency. Class I complexes are 'ionic' while Class II compounds are 'covalent' and the necessary enhancements to MM are derived respectively from 'ionic' LFT and the 'covalent' VB model. Naturally, many real molecules will fall somewhere between these two extremes. Ideally, a single model which can cope with both situations is required. Recent work suggests that the LFSE concept can be extended and modified to generate a new stabilisation energy term based on Burdett's Molecular Orbital Stabilisation Energy (MOSE) term [10] but without any metal valence p orbital contribution. This new model promises to provide a single MM-based framework for regular and irregular organometallic and classical complexes from across the entire transition series.

2. Complexes with open d shells

The most famous example of how the stereochemical activity of the d electrons can have a pronounced affect on molecular structure is the Jahn–Teller distortion of six-coordinate d^9 Cu^{2+} complexes. The ground state of a rigorously octahedral

d^9 CuL_6 complex is ^2E_g which is unstable with respect to a degenerate e_g vibration which distorts the system away from O_h symmetry. The details of the Jahn–Teller effect, vibronic coupling and the ensuing Mexican Hat potential energy surface have been described elsewhere [11] and will not be repeated here. In any event, only a simplified picture is required for the present purposes.

The majority of six-coordinate Cu^{2+} complexes display a pronounced tetragonal elongation which can be rationalised on the basis of Fig. 1. To first order, relative to the octahedral starting point, the important component of the degenerate Jahn–Teller active vibration corresponds to the equatorial ligands moving in by a distance δ and the axial ligands moving away by 2δ. This causes the e_g orbitals ($d_{x^2-y^2}$ and d_{z^2}) to split with $d_{x^2-y^2}$ rising and d_{z^2} falling in energy. Since there are two electrons in d_{z^2} and only one in $d_{x^2-y^2}$, there is a net electronic stabilisation of ΔE_{JT} driving the distortion. Countering the reduction in electronic energy is a rise in the vibrational energy as the structure moves away from octahedral. The stable configuration corresponds to the balance between these two competing factors.

Fig. 1 can also be used to explain why low-spin d^8 systems are invariably square planar since now the $d_{x^2-y^2}$ orbital is empty and the electronic stabilisation is $2\Delta E_{JT}$. The resulting additional tetragonal elongation is so severe that the axial ligands are displaced completely.

Deeth and Hitchman provided a simple theoretical analysis of Jahn–Teller distortions in such systems [11]. The electronic stabilisation energy term was based on simple LFT while the vibrational energies were estimated by interpolating the e_g force constant from analogous Ni^{2+} and Zn^{2+} species. This work formed the basis of the author's generalised approach to the direct inclusion of Ligand Field electronic effects for any coordination number and d configuration within a MM framework.

2.1. The ligand field stabilisation energy

Throughout the history of crystal field theory (CFT) and ligand field theory, it has been remarkable how often the ligand field stabilisation energy concept has

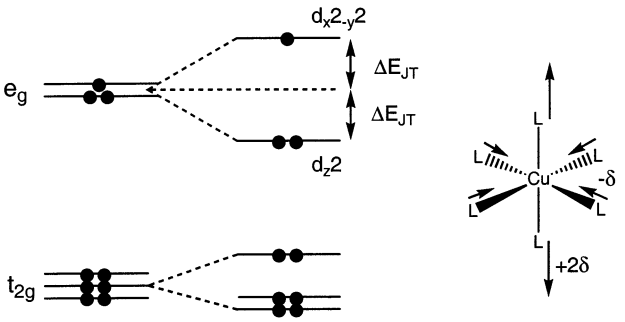

Fig. 1. Schematic representation of the electronic stabilisation energy, ΔE_{JT}, accompanying a tetragonal elongation of an octahedral d^9 Cu^{2+} complex.

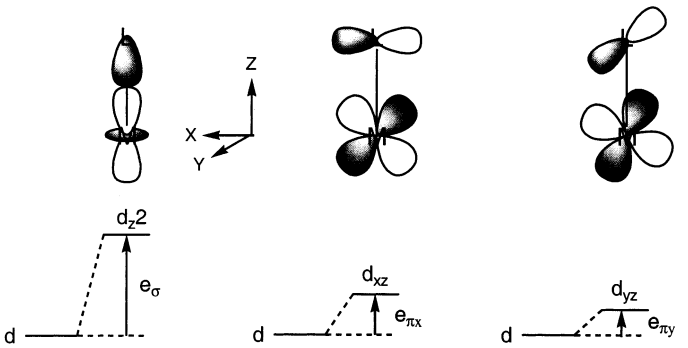

Fig. 2. Definition of the Cellular Ligand Field energy parameters e_σ, $e_{\pi x}$ and $e_{\pi y}$ in terms of the local d orbitals d_{z2}, d_{xz} and d_{yz}.

provided an insight into the structure and reactivity of coordination complexes. Some familiar examples include [12] (i) the 'double hump' variation of a range of experimental thermodynamic quantities such as the hydration enthalpies of the M^{2+} ions of the first transition series; (ii) site preferences for the tetrahedral and octahedral holes in spinels and (iii) the stability of octahedral complexes with d^3 and low-spin d^6 configurations. The difference between the LFSEs for ground state and models of the transition state (TS) for associative and dissociative ligand exchange/substitution at six-coordinate metal centres also gives some guides to the relative lability of certain d configurations and to the likely mechanism. Any general theoretical model for calculating the structures of TM species needs to account for the effects arising from the incomplete d shell. This will be implicit in a quantum mechanical model such as DFT. However, for an empirical scheme like MM, the simplest way to capture all the highly desirable features of the LFSE is to add a generalised LFT calculation directly onto the standard strain energy expression.

2.2. Generalised ligand field theory for computing the LFSE

The essential requirements for the general calculation of LFSEs is a model which is independent of coordination number and geometry and which can be parameterised at the level of individual M–L bonds to facilitate merging the LFSE contributions with the conventional bond-stretching terms from MM. This immediately precludes global parameterisation schemes and obliges us to employ a localised approach such as the angular overlap model (AOM) or the related cellular ligand field (CLF) method [13–15]. (The differences between the AOM and CLF approaches have been discussed extensively [16]. However, for our purposes, the models are essentially identical.)

The essence of the CLF scheme is the division of the space around the metal into separate 'cells' with each cell containing a single metal-ligand bond. The local perturbation of the d orbitals is then parameterised with respect to the local

bonding symmetry – σ, π*x* or π*y* as shown in Fig. 2. The local d orbitals interact with appropriate bonding functions and the subsequent energy changes are expressed in terms of the local e parameters e_σ, $e_{\pi x}$ and $e_{\pi y}$. By construction, if the M–L interaction describes ligand-to-metal donation, the relevant e parameter has a positive sign and the d orbital is destabilised. Conversely, for a ligand acceptor interaction, the e parameter is negative and the relevant d orbital is stabilised.

The total LF potential is then constructed as the sum of all the local contributions suitably modified to take into account the relationship between the orientation of the local M–L axis frame and the global reference frame. For example, a ligand aligned along the global *Z*-axis destabilises the d_{z^2} orbital by an energy equal to e_σ whereas a ligand on the *X*-axis contributes an energy change of only $1/4e_\sigma$. The remaining $3/4e_\sigma$ energy change is directed at the $d_{x^2-y^2}$ orbital.

Within the CLF (or AOM) scheme, the octahedral ligand field splitting, Δ_{oct}, for an ML_6 system is given by:

$$\Delta_{oct} = 3e_\sigma(L) - 4e_\pi(L) \tag{1}$$

In O_h symmetry, $d_{x^2-y^2}$ and d_{z^2} are degenerate. However, if all six ligands are different, the degeneracy is lifted. Hence:

$$E(d_{x^2-y^2}) = 3/4\{e_\sigma(L_{X+}) + e_\sigma(L_{Y+}) + e_\sigma(L_{X-}) + e_\sigma(L_{Y-})\} \tag{2}$$

$$E(d_{z^2}) = e_\sigma(L_{Z+}) + e_\sigma(L_{Z-}) + 1/4\{e_\sigma(L_{X+}) + e_\sigma(L_{Y+}) + e_\sigma(L_{X-}) + e_\sigma(L_{Y-})\} \tag{3}$$

In Eqs. (2) and (3) the notation L_{X+} signifies a ligand on the positive *X*-axis.

In general, it is necessary to construct the complete 5×5 LF potential matrix and diagonalise it to obtain the d orbital energies. As described by Burton et al. [6], these energies are expressed with respect to a 'Crystal Field' barycentre such that the sum of the d orbital energies is zero (Fig. 3). The d electrons are then placed in the correct orbitals, taking due note of the required spin state, and the LFSE evaluated.

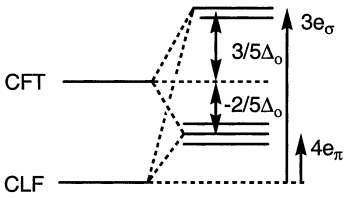

Fig. 3. A comparison of the d-orbital energy zeroes of the Crystal Field and Cellular Ligand Field models.

2.3. The LFMM method for electronically simple systems

A simple expression for the total MM strain energy, U_{total}^{MM}, is given by Eq. (4).

$$U_{total}^{MM} = \Sigma (E_b + E_\theta + E_\phi + E_{nb} + E_\varepsilon) \quad (4)$$

The terms on the right-hand side refer respectively to bond stretching, angle bending, torsional twisting, non-bonding interactions and electrostatic interactions. Eq. (4) represents a fairly minimal set of energy terms required to treat organic compounds, for example. More sophisticated expressions are certainly possible which employ additional terms and/or constraints, but Eq. (4) is sufficient for illustrative purposes.

Each term in Eq. (4) describes a penalty function representing the energy cost associated with the difference between some actual parameter value, say a bond length, and its 'ideal' value. Hence, for each type of bond, an 'ideal' bond length is defined and assigned a force constant to model the energy penalty for changing the bond length away from this ideal value. These molecular parameters may be defined a priori in a look-up table or derived algorithmically from a set of atomic parameters and together with the strain energy expression define the force field (FF).

In the LFMM scheme, Eq. (4) is augmented by the LFSE:

$$U_{total}^{LFMM} = \Sigma (E_b + E_\theta + E_\phi + E_{nb} + E_\varepsilon + LFSE) \quad (5)$$

Minimising U_{total}^{LFMM} requires the evaluation of the LFSE and its energy derivatives with respect to displacements of the metal and the ligand donor atoms. Finite difference derivatives are sufficiently accurate although this method is relatively time-consuming since each displacement involves a separate diagonalisation of the LF matrix. However, we have recently developed the algebra for analytical derivatives and will be implementing them in the near future.

2.3.1. Low-spin d^6 Co^{3+} complexes

As an illustrative example of how the LFMM method works, let us consider low-spin d^6 complexes of Co^{3+}. Such systems are invariably close to octahedral and consequently are amenable to a conventional MM treatment based on Eq. (4). In addition, this geometry is reinforced by the LFSE, which is a maximum for this symmetry and d configuration. Low-spin d^6 species are thus 'electronically simple' in that the LFSE favours a regular structure and the results of conventional MM can be exploited to parameterise the LFMM model.

Hancock has discussed MM calculations for six-coordinate Co^{3+} amine complexes and gives the 'ideal' Co–N distance as 1.925 Å and harmonic oscillator force constant of 2.00 mdyne $Å^{-1}$ [17]. The parameters of the LFMM can then be chosen to mimic this function, at least in the vicinity of the minimum.

The LFMM bond stretch term has both electronic, vibrational and non-bonding components, i.e. ligand–ligand 1,3 interactions. Since saturated N donors have no π bond, e_π is zero and so the LFSE is a function only of $e_\sigma(N)$.

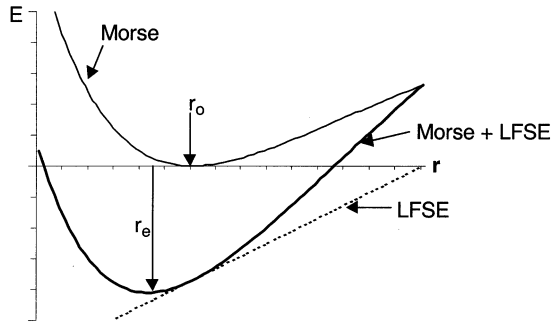

Fig. 4. The combination of the vibrational energy and the LFSE shifts the optimal M–L bond length, r_e, to shorter distances than the ideal value, r_0, used in the Morse function.

$$\mathrm{LFSE}(d^6,\ \text{low spin}) = -36/5\ e_\sigma(N) \tag{6}$$

The LFSE per ligand is one sixth of the total. By expressing $e_\sigma(N)$ as a function of the Co–N distance, r, the LFSE can also be written as a function of r. For simplicity, we may choose a simple linear function which yields the approximate $e_\sigma(N)$ value corresponding to 1/3 of the octahedral splitting derived from the d–d spectrum of, say, $[Co(NH_3)_6]^{3+}$ ($\Delta_{oct} \approx 23\ 000\ cm^{-1}$), at the relevant bond length of 1.96 Å and decreases to zero at a Co–N distance of, say, 2.55 Å (Eq. (7)).

$$e_\sigma(N) = 33\ 100 - 13\ 000r\ \mathrm{cm}^{-1} \tag{7}$$

The LFSE per ligand is thus:

$$\mathrm{LFSE}_{lig}(d^6,\ \text{low spin}) = -6/5(33100 - 13000r)\ \mathrm{cm}^{-1} \tag{8}$$

The LFSE becomes more negative as the bond length decreases so a conventional bond stretch term is used to prevent the molecule from collapsing in on itself. Since the LFMM model is targeted at electronically challenging metal centres, in particular Cu^{2+} where the tetragonal distortions can result in the axial and equatorial Cu–L distances differing by up to 0.7 Å even when L is the same is both cases, a Morse function (Eq. (9)) is a more suitable representation for the bond stretching potential energy curve.

$$E_b(\mathrm{Morse}) = D_0[1 - e^{-\alpha(r - r_0)}]^2 \tag{9}$$

The LFSE contribution to the bond stretch term inevitably means that the final M–L distance will be shorter than the 'ideal' value used in the Morse function (Fig. 4). This value corresponds to the M–L distance of a hypothetical complex where each d orbital has the same population — i.e. the d shell is spherical and the LFSE is zero — and any non-bonding interactions are absent.

In fact, the ideal bond length from the conventional MM treatment (1.925 Å) is also smaller than the observed Co–N distances (≈ 1.97 Å). The short Co–N distances in octahedral complexes result in N···N distances on the repulsive part of the ligand-ligand van der Waals energy surfaces. The increased steric crowding

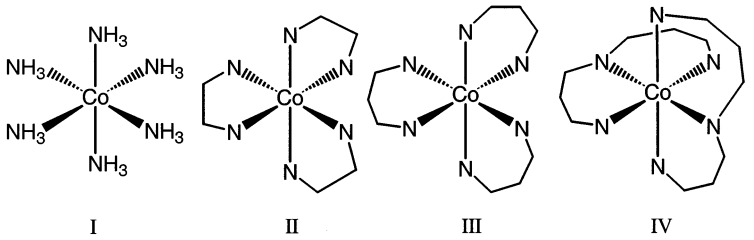

Fig. 5. Schematic representations of Co^{3+} amine complexes.

causes the observed bond length to be longer than the ideal value. Consequently, the Co^{3+} ion has been labelled 'hypersmall'.

It is straightforward to find a set of LFMM parameters which reproduces the position and curvature of the minimum from the harmonic oscillator treatment. The electronic term (Eq. (8)) is derived from experimental spectral measurements, the nitrogen non-bonding parameters are fixed at standard values and the Morse function parameters are adjusted [5]. For the present Co^{3+} amine complexes a comparison of theoretical and experimental results for the complexes shown in Fig. 5 is given in Table 1 where the dissociation energy, D_0, α and r_0 Morse function parameters are 75 kcal mol^{-1}, 0.45 and 2.663 Å, respectively.

The first conclusion is that the LFMM model gives as good agreement with the experimental Co–N distances as the conventional treatment. The second conclusion is that the bond angles calculated by the LFMM approach are in better agreement with experiment than that reported for conventional MM.

The LFMM angle-bend term (Eq. (5)) does not include any explicit N–Co–N term. This solves the so-called 'unique labelling' problem, i.e. that there are two possible bond angles of 90 and 180° but only one 'ideal' value can be entered into a simple harmonic oscillator expression. However, to recover the angular energy, explicit ligand–ligand 1,3 interactions are enabled for both the non-bonding and electrostatic terms. In addition, there is an implicit contribution to the N–Co–N angle from the LFSE. The $e_\sigma(N)$ value derived from experimental spectroscopic data apparently provides a good description of the angular potential around the metal centre.

Table 1
Selected geometrical data for the Co^{3+} amine structures shown in Fig. 5

Complex	Calc. *observed*			
	I	II	**III**	**IV**
Co–N (Å)	1.96 *1.96*	1.96 *1.96*	1.99 *1.98*	1.99 *2.00* 2.02 *2.04*
N–Co–N (°)	90 *90* 180 *180*	90 *91* 176 *176*	90 *90* 179 *178*	90 *90* 177 *175*

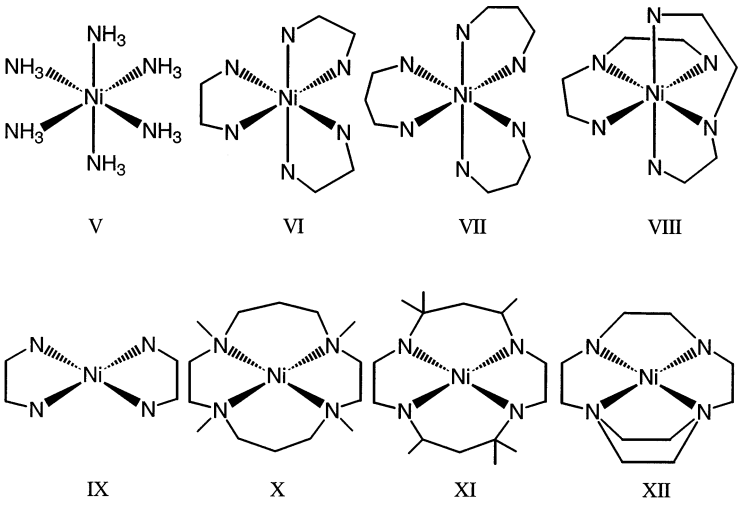

Fig. 6. Schematic representations of six-coordinate high-spin and four-coordinate low-spin d^8 Ni^{2+} amine complexes.

2.3.2. High spin and low spin Ni^{2+} complexes

In the LFMM model, there are multiple, linearly dependent contributions to the M–L bond length-the LFSE, the Morse function and non-bonding interactions-so there is a infinite number of solutions. However, this turns out to be an advantage since it allows us to do more with the LFMM parameterisation. For example, it is possible to choose a single set of Ni–N LFMM parameters which models both low-spin and high-spin complexes of d^8 Ni^{2+} [6]. This feature of the LFMM model contrasts with more conventional MM approaches where two different sets of FF parameters are required [17]. In more complex systems such as the Fe-porphyrins, separate MM2 parameters have been proposed for each spin state, coordination number and metal oxidation state [18].

For Ni^{2+} amine species, Hancock reports separate Ni–N parameters for high-spin and low-spin complexes. Within the LFMM scheme, a single set of Ni–N parameters was found which simultaneously reproduced both curves simply by altering the population of the d orbital to reflect the desired spin state. The e_σ values employed to compute the LFSE were based on a number of CLF analyses of the d–d spectra for various Ni-amine complexes which suggest, at least for an equatorial donor, that the CLF Ni–N e_σ parameter depends linearly on the bond distance over the range 2.0 to 2.3 Å and the best-fit straight line through these empirically defined data points was employed in the LFMM modeling [19]. A selection of calculated and observed structural data for the complexes shown schematically in Fig. 6 is shown in Table 2.

As mentioned above, there is a large driving force for the tetragonal elongation of a hypothetical low-spin octahedral Ni^{2+} complex. The LFMM parameters give axial and equatorial bond lengths for a model 'bare ligand' NiN_6 species of 2.78

and 1.90 Å, respectively. The LFMM model predicts a bond length difference of nearly 0.9 Å and it is easy to imagine that the axial ligand would simply be displaced to yield the final square planar geometry.

2.4. The LFMM model for electronically difficult metals

Complexes of the d^9 Cu^{2+} ion present perhaps the greatest challenge for MM schemes. Not only are they intrinsically flexible or 'plastic', displaying a wide range of coordination numbers and geometries, but they generally deviate significantly from ideal structures due to the Jahn–Teller effect. Both angular and bond length distortions are common. Thus, the Cu–L distance may vary over a range of 0.5–0.7 Å depending on the site of coordination. For example, a typical distance for an equatorially coordinated amine nitrogen is around 2.0 Å while axial Cu–N distances are around 2.4–2.5 Å. However, these bond length variations arise from an electronic effect which is captured by the LFSE term. The LFMM scheme is thus unique among empirical models in that it automatically generates Jahn–Teller distorted structures [7].

2.4.1. Cu^{2+} complexes and multiple coordination numbers

LFMM calculations have been reported for several 4-, 5- and 6-coordinate Cu^{2+} amine complexes [6]. The LFSE term was derived from earlier CLF calculations of the d–d spectra for Cu^{2+} amine complexes and hence the LFMM parameters are approximately the same as those derived from spectroscopic analyses. It turns out that the e_σ term for Cu–N bonding is essentially the same as that for Ni–N. In fact, the only significant difference between the Cu–N and Ni–N parameters is the number of d electrons. A selection of observed and calculated structural data for the complexes shown in Fig. 7 is given in Table 3.

In general, the comparison between experiment and the LFMM geometries is very good. However, some care should be taken concerning exactly what we should be trying to reproduce. X-ray crystallographic studies are the usual source of experimental geometrical data but these can be quite unreliable as a basis for developing parameters for Cu^{2+} species. The problem is especially marked for five- and six-coordinate species.

Table 2
Selected geometrical data for the Ni^{2+} amine structures shown in Fig. 6

Complex	Ni–N (Å)	*cis*-N–Ni–N (°)	*trans*-N–Ni–N (°)
V	2.12 *2.13*	90 *90*	180 *180*
VI	2.11 *2.13*	81 *82*	172 *172*
VII	2.12 *2.15*	86 *87*	175 *176*
VIII	2.04 *2.06* 2.14 *2.15*	82 *82*	168 *167*
IX	1.93 *1.92*	87 *86*	180 *180*
X	1.97 *1.98*	91 *91*	167 *169*
XI	1.97 *1.96*	90 *90*	180 *180*
XII	1.84 *1.87*	90 *90*	169 *169*

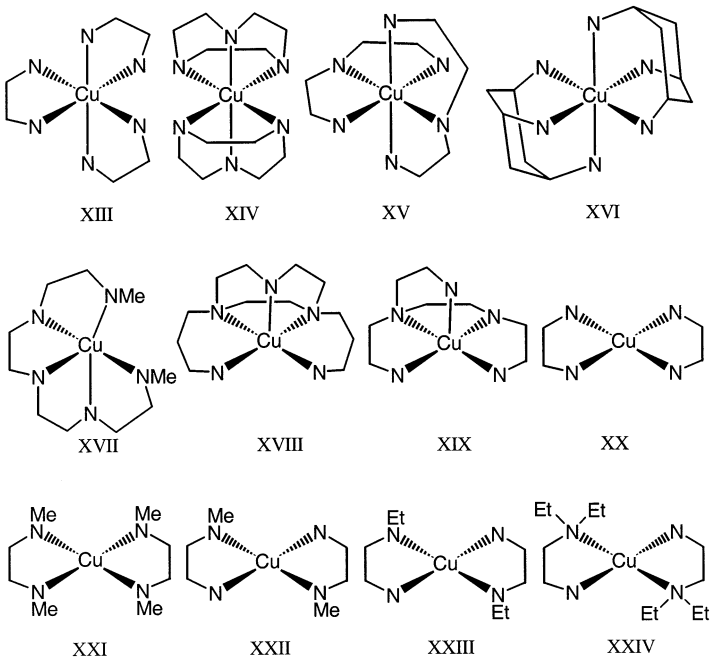

Fig. 7. Schematic representations of six-, five- and four-coordinate Cu^{2+} amine complexes.

Table 3
Selected geometrical data for the Cu^{2+} amine structures shown in Fig. 7

Complex	Cu-N [a] (Å)	*cis*-N–Cu–N (°)	*trans*-N–Cu–N (°)
XIII	1.97 *2.00* 2.03 *2.08* 2.46 *2.41*	80 *81*	170 *170*
XIV	1.96 *2.06* 2.13 *2.07* 2.29 *2.32*	81 *81*	177 *178*
XV	2.02 *2.05* 2.10 *2.08* 2.41 *2.41*	80 *81*	164 *166*
XVI	2.01 *2.07* 2.28 *2.35*	89 *87*	180 *180*
XVII	1.96 *2.01* 2.10 *2.03* 2.37 *2.16* 2.00 *2.02* 2.13 *2.09*	85 *85* 111 *105* 115 *112* 86 *85* 96 *100*	169 *168* 141 *140*
XVIII	2.03 *2.03* 2.03 *2.06* 2.32 *2.25* 2.08 *2.08* 2.03 *2.05*	91 *90* 102 *102* 78 *82* 86 *86* 80 *84*	175 *173* 173 *165*
XIX	1.95 *2.01* 2.18 *2.09* 2.39 *2.09* 2.08 *2.04* 2.05 *2.01*	83 *86* 109 *117* 82 *86* 116 *105* 98 *96*	131 *128* 165 *170*
XX	2.03 *2.02*	84 *84*	180 *180*
XXI	2.05 *2.06*	85 *85*	170 *180*
XXII	2.00 *2.01* 2.04 *2.06*	85 *86*	180 *180*
XXIII	2.00 *2.01* 2.04 *2.03*	85 *85*	180 *180*
XXIV	1.96 *2.01* 2.08 *2.08*	86 *85*	180 *180*

[a] Averaged over *trans*-related ligands

For six-coordinate Cu^{2+} complexes, the averaging that can accompany a static or dynamic Jahn–Teller effect can mask the true, underlying geometry. For example, the nitrate salt of $[Cu(1,3,5\text{-triaminocyclohexance})_2]^{2+}$ (**XVI** in Fig. 7) ion has six apparently equal bond Cu–N bond lengths. However, the d–d spectrum shows more than the single transition expected if the system truly were octahedral. In fact, the spectrum is essentially identical to that from the perchlorate salt which contains a typical elongated copper centre. In both cases, the actual geometry is tetragonally elongated but the diffraction experiment does not always detect this. The upshot is that the lowest energy systems correspond to those with the largest elongations and this idea has dictated the choice of experimental system to use for developing LFMM parameters.

Pentacoordinate complexes also cause difficulties [20]. These species are intrinsically flexible with only a small energy change between the extreme geometries of trigonal bipyramidal and square pyramidal. However, when this is coupled with the peculiar electronic effects of the d^9 configuration, large bond length changes are superimposed on the changes in angular geometry. For example, a typical Cu–N distance for an axial tbp site is around 2.0 Å or while the same ligand in the apical site of a square pyramid will have a bond length around 2.4 Å. As shown in Fig. 8 these structural changes relate to the orientation of the hole in the d shell. Indeed, the difference between the energy computed for an isolated complex with the geometry observed in the crystal structure and the fully LFMM optimised geometry is less than 3 kcal mol^{-1} for $[Cu(2,5,8,11,14\text{-pentaazapentadecane})]^{2+}$ (**XVII**), $[Cu(1,4\text{-di(3-aminopropyl)-1,4,7-triazacyclononane})]^{2+}$ (**XVIII**) and [Cu(N,N-dimethylaminoethyl)amine]$^{2+}$ (**XIX**) which implies that the relatively subtle effects of crystal packing could have a profound affect on the observed structure. Therefore, it is unrealistic to expect MM calculations on isolated complexes always to reproduce the structures observed in a crystal.

Square-planar four-coordinate Cu^{2+} complexes are the easiest to model since they represent the extreme of the Jahn–Teller distortion. This conclusion is borne out by the data in Table 3 and by the numerous attempts to employ conventional MM to copper systems [21]. However, there are still lattice effects. For example, the bite angles for the Br^- and NO_3^- salts of $[Cu(1,3\text{-diaminocyclohexane})_2]^{2+}$ change by 6° due to subtle changes in the ligand conformations. Nevertheless, the impor-

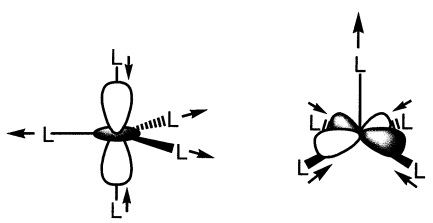

Fig. 8. The stereochemical activity of the hole in the d shell for five-coordinate Cu^{2+} species. Left: in trigonal bipyramidal symmetry, the hole is in d_{z^2} and encourages short axial and long equatorial bonds. Right: in square pyramidal symmetry, the hole is in $d_{x^2-y^2}$ which encourage short equatorial and long apical bonds.

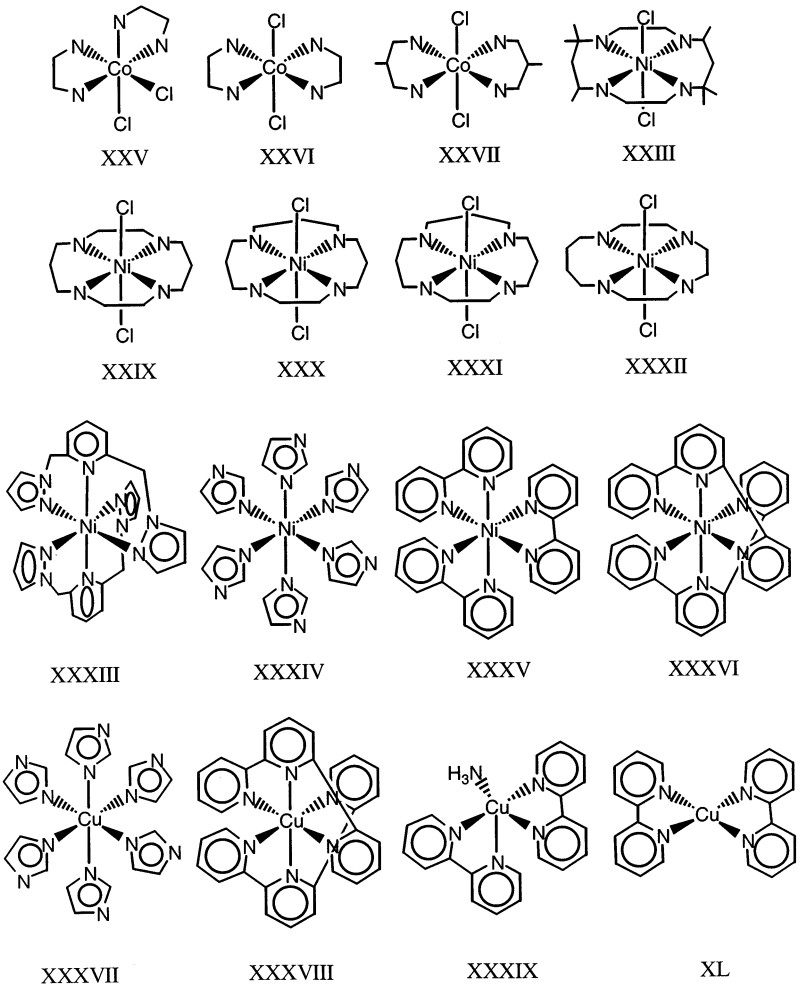

Fig. 9. Schematic representations of mixed ligand and imine complexes of Co^{3+}, Ni^{2+} and Cu^{2+}.

tant result is that the LFMM model reproduces the structures of four-, five- and six-coordinate systems with a single set of parameters.

2.4.2. LFMM calculations on complexes with π-donor ligands

The LFMM parameterisation has been extended to imine and chloro complexes of Co^{3+}, Ni^{2+} and Cu^{2+} including complexes containing mixtures of these donors as shown in Fig. 9 [5]. In general, the form of the functions used to estimate e_σ and e_π as a function of bond length are derived by comparison with available CLF parameters determined from the analyses of d–d and/or magnetic data. However, there is a reasonably high degree of linear dependency in the LFMM parameterisation so it is certainly not mandatory that the actual CLF parameter values are

precisely those which would be deduced spectroscopically. To that end, it is possible to compute the structures of complexes which contain ligands formally capable of metal–ligand π bonding without any explicit CLF e_π parameters.

This σ-only model was applied to a series of complexes with imine ligands. With only a few exceptions, the LFMM model gives excellent agreement with experimental structures with root mean square deviations in M–L bond lengths and L–M–L angles of around 0.03 Å and 3°, respectively. The most significant discrepancies are for $[Cu(2,2'\text{-bipyridyl})_2(NH_3)]^{2+}$ (**XXXIX**), $[Cu(2,2',2''\text{-terpyridyl})_2]^{2+}$ (**XXXVIII**) and $[Cu(2,2'\text{-bipyridyl})_2]^{2+}$ (**XL**). The error for the first complex is presumably due to the problems associated with pentacoordinated structures and is therefore not serious. However, **XXXVIII** is predicted to be tetragonally compressed and the calculated structure of **XL** is in poor agreement with experiment. The former problem seems to be associated with the FF parameters. There is a fine balance between tetragonal compression and elongation and indeed the Ni^{2+} terpyridyl complex (**XXXVI**) is also compressed with a 0.15 Å difference between the equatorial and axial bond lengths. Evidently, the current FF is not properly balanced and is unable to overcome the tendency for a compressed structure. The problem with **XL** can be traced to the lack of electrostatic interactions.

The interligand interactions in $[Cu(2,2'\text{-bipyridyl})_2]^{2+}$ prevent the two ligands from being coplanar. The geometry around the Cu centre is therefore flattened tetrahedral. As described above, the LFSE term for a four-coordinate d^9 system naturally favours a planar geometry so some additional term is required to distort the structure towards a tetrahedron. Given that 1,3-ligand–ligand interactions are explicitly included in the LFMM model, one could increase the repulsive term of the nitrogen non-bonding energy but a very large increase is required. Alternatively, an explicit π bonding contribution to the LFSE could be added. This encourages a tetrahedral distortion but e_π has to exceed e_σ for any significant effect to be observed. The best option is to consider nitrogen-nitrogen electrostatic interactions. A metal charge of 0.5 and nitrogen charges of -0.41, in conjunction with modifications to the Morse function parameters, resulted in excellent agreement with experiment.

We are left then to ponder whether π-bonding makes a significant contribution to the LFMM model. Apparently, for the type of system considered so far, explicit π parameters are not required. However, it is difficult to imagine how this situation can be general. For example, dynamic Jahn–Teller distortions are generally cited as being responsible for the shoulder on the d–d absorption band of d^1 $[Ti(H_2O)_6]^{3+}$ and for the splitting of the excited ^5E_g state in high spin d^6 complexes of Fe^{II} and Co^{III}. These features arise from a Jahn–Teller instability in the t_{2g} orbitals which cannot be captured in a σ-only scheme. Further work is required to explore the extent to which explicit π parameters should be included in the LFMM scheme.

2.4.3. Cu^{2+} catalysts for Diels–Alder reactions

Copper complexes of oxazoline ligands have been reported to be efficient enantioselective catalysts for two-point Diels–Alder coupling reactions. As is common in catalytic reactions, the structures of intermediates including the actual

catalyst often cannot be determined. A series of spiro oxazoline ligands (Fig. 10) gave increasingly high enantiomeric excesses with increasing ring size which correlated with a decreasing angle, Ψ, in the isolated ligands (Fig. 10). It was presumed that the variation in Ψ would also influence the bite angle at the Cu^{2+} centre. To test this hypothesis, a set of LFMM parameters was developed for Cu–oxazoline and Cu–pyridineoxazoline complexes [22]. As with previous LFMM studies of Cu^{2+} systems, a σ-bonding-only approach (with 1,3 electrostatic interactions) correctly reproduces the coordination geometries even though the ligands are formally capable of metal–ligand π bonding.

X-ray crystal structures of five representative compounds formed the basis for parameter development. Only minor modification of the existing Cu^{2+}–imine parameters was required to generate an acceptable fit between theory and experiment. Overlaid structures are shown in Fig. 11 and selected structural data are collected in Table 4.

The calculated structures for diaqua complexes of the spiro inbox ligands show a good correlation between the ligand angle, Ψ, in the complex and the bite angle Φ at the metal. These data also correlate well with the observed selectivities for the Diels–Alder coupling of cyclopentadiene with an oxazolidinone capable of two-point binding to a copper centre (Table 5). A significant feature of the LFMM calculations is the prediction of a pronounced tetrahedral distortion of these four-coordinate species. The dihedral angle between the N_2Cu and O_2Cu planes is about 20°. This twist is believed to be a key factor for understanding the sense of chiral induction in these systems.

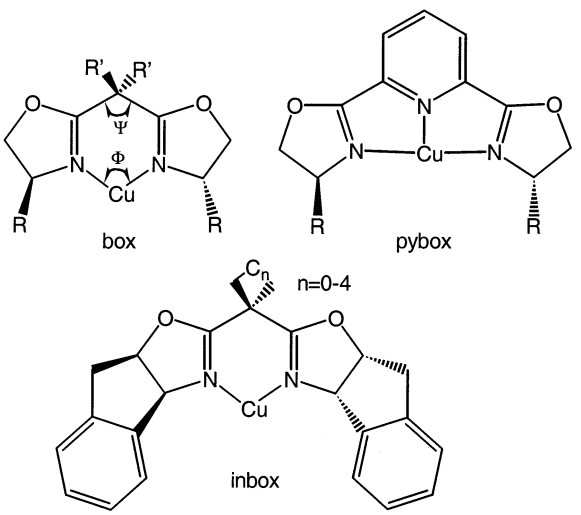

Fig. 10. Schematic representations of oxazoline–ligand complexes.

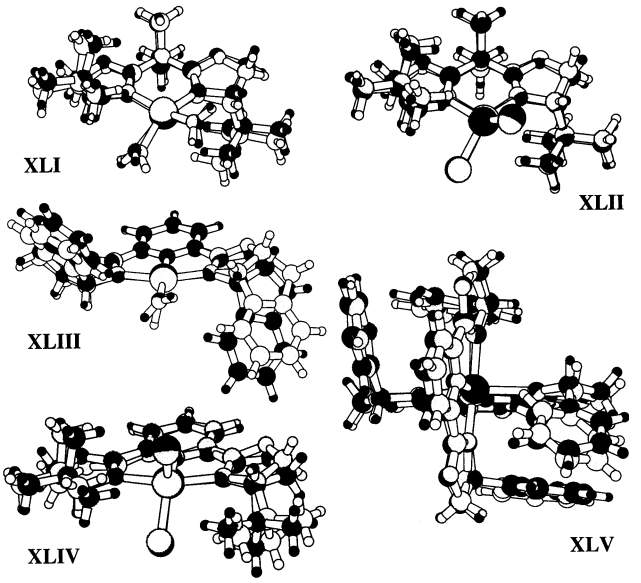

Fig. 11. Comparison of the observed (white) and calculated (black) structures of Cu^{2+} oxazoline–complex.

Table 4
Metal–ligand bond lengths for the Cu^{2+} oxazoline structures shown in Fig. 11

	Calc. observed			
	$Cu–N_{ox}$	$Cu–N_{py}$	Cu–O	Cu–Cl
XLI	1.97 *1.94*		2.02 *1.98*	
XLII	2.00 *1.98*			2.20 *2.23*
XLIII	2.07 *2.11*	1.98 *2.01*		2.33 *2.27*
XLIV	2.00 *2.05*	1.96 *1.94*	1.86 *1.96*	
XLV	2.06 *2.05* 2.07 *2.08* 2.27 *2.30* 2.34 *2.40*	1.90 *1.96* 2.00 *2.02*		

Table 5
Selected calculated geometrical parameters for diaqua complexes of spiro inbox ligands (see Fig. 10) and the experimental selectivities for the Diels–Alder reaction between cyclopentadiene and an oxazolidinone

Ligand	Φ (°)	Ψ (°)	χ (°)	Cu–N	$Cu–OH_2$	*endo*(*R*)/(*S*)	*endo*:*exo*
Cyclopropyl-inbox	97.7	120.6	19	2.01	2.01	53:1	44:1
Cyclobutyl-inbox	96.3	115.8	18	1.99	2.01	24:1	38:1
Cyclopentyl-inbox	95.7	113.2	20	1.99	2.01	18:1	37:1
Cyclohexyl-inbox	94.9	111.5	22	1.97	2.01	11:1	26:1

2.5. Other approaches for Werner complexes

Hambley and Comba have developed a conventional MM scheme parameterised for certain Cu^{2+} complexes [23]. However, it does not contain a general d-electron energy and thus individual ligands have separate parameter sets depending on whether they occupy, say, axial or equatorial sites.

However, for the particular case of six-coordinate, tetragonal Cu^{2+} systems, a simplified energy constraint based on Lagrangian multipliers has been implemented. The term is derived from the LFSE for a tetragonal distortion of an octahedral CuN_6 system and the energy profile for each of the three possible axes of distortion must be mapped out to determine which has the lowest overall energy [24].

As mentioned above, the value of e_σ depends on the M–L distance. This feature has been exploited in an attempt to use the MM structure for a subsequent calculation of various ligand field properties such as d–d transition energies and electron paramagnetic resonance g-values. The LF calculations are based on the AOM. While this model does not fall into the remit of this review per se, its application revealed an apparent discrepancy between theory and experiment for certain types of strained system. This error was attributed to 'misdirected valency' in that for bite angles which deviate significantly from 90° the ligand lone pairs cannot interact as effectively with the metal d orbitals. The remedy was to modify the expression for e_σ using a $\cos^6\theta$ angular dependence [25].

In principal, an explicit misdirected valence term could be added to the LFMM model. There are many examples of CLF analyses demonstrating the extent of misdirected valence [26–28]. The effect is accommodated by defining a new energy parameter $e_{\pi\sigma}$ which reflects the extent to which the source of the local ligand field potential lies off the M–L vector. However, given the empirical nature of the LFMM scheme and that there is as yet no demand that the CLF parameter values underlying the LFSE calculation should be identical to those determined from spectroscopic and/or magnetic measurements, $e_{\pi\sigma}$ parameters have not been implemented.

3. Organometallic compounds, sd″ hybrids and d–s mixing

Certain organometallic compounds like the binary metal carbonyls have regular structures. The simplest angular potential energy function in MM is based on a quadratic equation. This is unsuitable for, say, $Cr(CO)_6$ since the L–M–L angle can take more than one 'ideal' value. One response to this 'unique labelling' problem is to use a Fourier transform which has multiple minima corresponding to the observed L–M–L angles, e.g. 90 and 180° in square planar or octahedral symmetry.

The angular geometries of certain organometallic species are even more complicated. For example, WMe_6 is formally a W^{6+} d^0 species and is therefore expected to display a regular octahedral geometry at the metal. However, the actual structure is a distorted trigonal prism [29] analogous to that shown for WH_6 in Fig. 12(a). Landis and co-workers have developed the Hypervalent-VALBOND (HV-VB) MM

method to account for this and related structures [9,30]. The central idea is the development of angular potential energy functions based on the properties of sd^n hybrid orbitals. For sd and sd^2 hybrids, the idealised interhybrid bond angles are 90°. However, for sd^3 to sd^5 hybrids, there are two ideal bond angles -63 and 117° for sd^5. The angles between the methyl groups in WMe_6 are found to be very close to these values. For the all-hydride system WH_6, there are three other molecular geometries, which can accommodate the 63 and 117° angular preferences of sd^5 hybridisation (Fig. 12). All four have been located using quantum chemical calculations and the resulting structures and energies are in good agreement with the HV-VB predictions. The HV-VB MM model has been applied to a variety of transition metal hydride, alkyl and aryl compounds with excellent results.

In the HV-VB MM model, the deviations away from regular structures depend explicitly on the mixing between the valence d and s orbitals on the metal. Therefore, to emulate this within the LFMM framework requires an s-orbital contribution to the stabilisation energy term. It is already well-known that s-orbital contributions in the form of so-called 'd–s mixing' are required for certain coordination complexes. For example, the energy of the d_{z^2} orbital in planar $[CuCl_4]^{2-}$ is about 6000 cm^{-1} higher than predicted by simple LFT [31]. Within the AOM/CLF framework, the discrepancy can be remedied either by adding an explicit s orbital to the basis set or by adding s-orbital contributions to the existing ligand field matrix elements. The two approaches have different parameters but there is a direct mapping between them and either approach can be used.

The d–s mixing term implicitly models sd^n hybridisation in a similar way to an Extended Hückel Molecular Orbital (EHMO) calculation with the metal valence p orbital removed. For WH_6, the hydrogen 1s orbitals and their overlaps with metal functions in the EHMO scheme are implicitly treated by e_σ parameters in the CLF model. Indeed, one could conceive of modelling the metal–ligand interaction wholly within the EHMO framework. However, as with other hybrid QM/MM schemes, complete ligands would be required and the issue of how to treat the

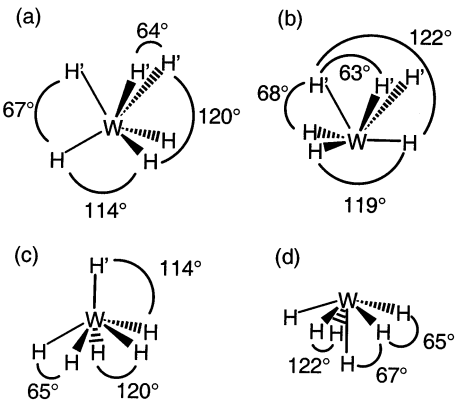

Fig. 12. Schematic representations of calculated structures of WH_6.

'quantum/classical' boundary would have to be addressed. For example, a PPh_3 ligand could be modelled with PH_3 in the EHMO part while the surrounding MM part would require parameters for P–C interactions. Since the quantum part of the LFMM approach is effectively just the metal atom, the boundary is simply the metal–ligand bond which is easy to handle.

The LFMM scheme with d-s mixing requires an additional caveat when applied to organometallic species like WH_6. Formally, WH_6 is a d^0 compound and, as such, has a zero LFSE. However, following Burdett [10], we recognise that this relates to the choice of d-orbital energy zero. The conventional definition of the LFSE relates to the original crystal field theory barycentre which requires that the d-orbital energies sum to zero. In contrast, the CLF energy zero is defined such that the sum of the d-orbital energies equals the sum of the CLF parameters. Thus, for an octahedral $[M(NH_3)_6]^{n+}$ complex where e_π is zero ($\Delta_{oct} = 3e_\sigma$), the energy of the t_{2g} orbitals would be $-2/5\ \Delta_{oct}$ ($-6/5\ e_\sigma$) relative to the CFT barycentre but zero relative to the CLF energy zero.

Both energy zeroes give identical stabilisation energies for d^n configurations. Consider the 'double hump' variation of, say, the hydration enthalpies of the M^{2+} cations of the first transition series. The difference between the experimental enthalpy and the point on the line interpolated between the values for those ions where the LFSE is zero (Ca^{2+}, Mn^{2+} and Zn^{2+}) correlates very well with the LFSE derived from spectroscopic measurements of Δ_{oct}. The point on the interpolated line thus corresponds to a spherically symmetric d shell, i.e. one in which all the d-orbitals have identical populations. Thus, for a d^1 $[M(NH_3)_6]^{n+}$, where the LFSE is $-6/5\ e_\sigma$ relative to the CFT barycentre, the t_{2g}^1 energy is zero but the spherically symmetric configuration with 1/5 of an electron in each d orbital is $1/5(0+0+0+3e_\sigma+3e_\sigma) = 6/5e_\sigma$ higher. Thus the stabilisation is $-6/5e_\sigma$.

The problem with WH_6 is that, as a formally d^0 complex, there is no LFSE. However, Burdett recognised that, to first order, the energy changes of the anti-bonding metal d (and s and p) orbitals were mirrored by equal and opposite energy changes in the symmetry matching bonding MOs as shown schematically in Fig. 13 for a hypothetical octahedral MH_6 system. He defined the Molecular Orbital Stabilisation Energy as:

$$\mathrm{MOSE} = -2\Sigma\ \varepsilon(\phi_i) + \Sigma\ \rho(\phi_i)\varepsilon(\phi_i) \tag{10}$$

where ϕ_i are the metal s, p and d orbitals of energy $\varepsilon(\phi_i)$ and containing $\rho(\phi_i)$ electrons.

The MOSE is therefore non-zero even for a formally d^0 system. Hence, given that Landis's HV-VB model demonstrates that the structures can be obtained based only on sd^n hybrids — i.e. the p orbitals are not required — the LFMM scheme with d–s mixing and the MOSE provides a framework for modelling organometallic compounds. Preliminary investigations of the structure of WH_6 support this contention and further results will be reported in due course. In fact, the MOSE could be employed for Werner-type complexes as well. The additional energy arising from the occupied bonding MOs would add a spherical contribution to bond shortening which would require a compensating adjustment of the Morse function bond stretch term.

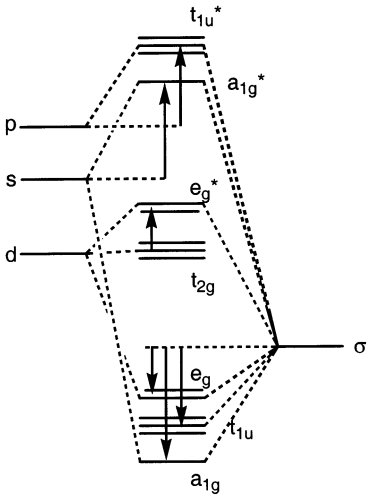

Fig. 13. Simplified MO diagram for hypothetical octahedral MH_6 complex. To first order, the energy rise of the anti-bonding MOs (up arrows) is equal and opposite to the fall of the bonding MOs (down arrows).

4. The LFMM model and transition states

As mentioned in Section 2.1, the LFSE concept has been successfully applied to a whole range of structural and thermodynamic properties of transition metal complexes. Of particular interest is the attempt by Basolo and Pearson to rationalise the reactivity of metal complexes in terms of the crystal field contribution to the overall activation energy. By calculating the change in CFSE for model dissociative and associative processes, they provided some qualitative guidance to the likely mechanism of substitution/exchange and the relative lability as a function of the d configuration. However, since the actual transition state structures were unknown they were obliged to guess model structures and consequently the correlation between theory and experiment is not perfect.

In contrast, Density Functional Theory calculations for some exchange reactions at planar d^8 centres give an accurate picture of the structure and relative energy of the transition state. For example, the TS for chloride exchange at $[PdCl_4]^{2-}$ [32] and water exchange at $[Pd(H_2O)_4]^{2+}$ [33] are shown in Fig. 14. The structures cannot be rigorously tbp structure since this does not correspond to a true first-order saddle point. However, the true structures are energetically and structurally quite close to tbp. Note that the 'axial' Pd–L distances are significantly shorter than the 'equatorial' bond lengths. This 'distortion' contrasts with the VSEPR prediction of longer axial bonds in tbp symmetry but correlates with the stereochemical activity of the low-spin d^8 configuration. In tbp symmetry, d_{z^2} is empty while the remaining d orbitals are filled. The reduced repulsion of the ligand electrons along the Z-axis permits the axial ligands to approach closely while the equatorial groups move away to compensate. This structure maximises the LFSE and should therefore be amenable to modelling within the LFMM approach.

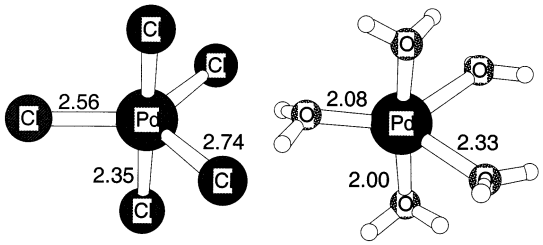

Fig. 14. DFT optimised transition state structures for chloride exchange on $[PdCl_4]^{2-}$ and water exchange on $[Pd(OH_2)_4]^{2+}$.

It is possible to develop a set of LFMM parameters for each of $[PdCl_4]^{2-}/Cl^-$ and $[Pd(H_2O)_4]^{2+}/H_2O$ which simultaneously reproduces the ground state structure of the planar starting material and the structure and relative energy of a five-coordinate TS model (Table 6) [4]. However, further DFT and LFMM work is required to explore how general and transferable the parameters are.

5. Conclusions

The stereoelectronic effects of the metal d and s electrons can cause severe departures from regular geometries. The d-electron effects are especially marked in more ionic Werner-type complexes and can be explained in terms of a balance between ligand–ligand interactions and the classical LFSE. By incorporating the LFSE directly into the calculation, the LFMM model is able automatically to account for the Jahn–Teller distortions of six-coordinate Cu^{2+} complexes using a single set of parameters. This contrasts with more conventional MM treatments which define separate parameters for short and long bonds. The LFMM model also reproduces the ~ 0.2 Å bond shortening accompanying the change from high to low spin in Ni^{2+} amine complexes, again with a single set of Ni–N parameters. The LFMM has been parameterised for amine, imine and chloro complexes of Co^{3+}, Ni^{2+} and Cu^{2+} and displays useful accuracy. However, while it is easy to incorporate the LFSE into conventional MM, significantly more work is required to develop a comprehensive modelling tool for Werner-type complexes.

The unusual geometries of certain covalent organometallic compounds, notably hydrides, alkyls and aryls, have been explained based on Valence Bond sd^n hybrids,

Table 6
Calculated bond lengths and energies for approximate tbp transition state models

L	Pd–L		$Pd–L_{ax}$		$Pd–L_{eq}$		$E^{\ddagger}$	
	LFMM	DFT	LFMM	DFT	LFMM	DFT	LFMM	DFT
Cl	2.33	2.31	2.28	2.30	2.62	2.64	141	143
H_2O	2.03	2.01	1.96	1.98	2.26	2.28	−6	−7

i.e. the metal p orbitals are not required. The special features of sd^n hybrids can also be captured within the LFMM framework by adding s-orbital contributions to the ligand field potential matrix elements (d–s mixing) and redefining the stabilisation energy analogously to Burdett's Molecular Orbital Stabilisation Energy. This allows the LFMM model to be used to calculate an electronic stabilisation energy term even for formally d^0 compounds like WH_6. Preliminary results show that in the absence of d-s mixing the LFMM scheme predicts a regular octahedral compound but once d–s mixing is included, the desired distorted trigonal prism structure is obtained.

The LFMM scheme can even predict transition state structures and energies at least for those systems where the LFSE contribution to the activation energy is significant, e.g. ligand exchange/substitution at planar d^8 centres. The LFMM model thus represents a viable platform for modelling transition metal compounds spanning the chemistries of the entire transition series.

But is the LFMM scheme worth developing further? With faster computers and the advent of sophisticated hybrid methods where the metal centre can be treated quantum mechanically, what is the future of simple but highly parameterised schemes like the LFMM model? Ultimately, I believe the question comes down to the speed of the calculation. The LFMM model is orders of magnitude faster than any comparably accurate QC method. Hence there will always be a place for such schemes simply by looking at larger and larger systems or, more significantly, at dynamic processes. Molecular dynamics based on quantum mechanics or even a hybrid quantum/classical scheme is still a formidable challenge and likely to remain so. Empirical schemes will remain valuable providing the physical basis of the methods are sound. Since the LFMM approach captures the important steric and electronic effects around the metal, it significantly extends the range of systems to which it applies and I believe it is worth the future investment.

Acknowledgements

The author acknowledges the financial support of the Engineering and Physical Sciences Research Council and the University of Warwick.

References

[1] M.R. Bray, R.J. Deeth, V.J. Paget, Prog. React. Kinetics 21 (1996) 169.
[2] R.J. Deeth, Struct. Bonding 82 (1995) 1.
[3] P. Comba, Coord. Chem. Rev. 182 (1999) 343.
[4] R.J. Deeth, I.J. Munslow, V.J. Paget, NATO ASI Series 3/41 (1997) 77.
[5] R.J. Deeth, V.J. Paget, J. Chem. Soc. Dalton Trans. (1997) 537.
[6] V.J. Burton, R.J. Deeth, C.M. Kemp, P.J. Gilbert, J. Am. Chem. Soc. 117 (1995) 8407.
[7] V.J. Burton, R.J. Deeth, J. Chem. Soc. Chem. Commun. (1995) 573.
[8] R.J. Deeth, M. Gerloch, Inorg. Chem. 24 (1985) 4490.
[9] C.R. Landis, T. Cleveland, T.K. Firman, J. Am. Chem. Soc. 120 (1998) 2641.

[10] J.K. Burdett, Molecular shapes: theoretical models of inorganic stereochemistry, Wiley, New York, 1980.
[11] R.J. Deeth, M.A. Hitchman, Inorg. Chem. 25 (1986) 1225.
[12] D.F. Shriver, P.W. Atkins, in: Inorganic Chemistry, third ed., Oxford University Press, Oxford, 1999.
[13] D.E. Richardson, J. Chem. Ed. 70 (1993) 372.
[14] M. Gerloch, R.G. Woolley, Prog. Inorg. Chem. 31 (1983) 371.
[15] R.G. Woolley, Mol. Phys. 42 (1981) 703.
[16] A.J. Bridgeman, M. Gerloch, Prog. Inorg. Chem. 45 (1997) 179.
[17] R.D. Hancock, Prog. Inorg. Chem. 37 (1989) 187.
[18] H.M. Marques, O.Q. Munro, N.E. Grimmer, D.C. Levendis, F. Marsicano, G. Pattrick, T. Markoulides, J. Chem. Soc. Faraday Trans. 91 (1995) 1741.
[19] R.J. Deeth, C.M. Kemp, J. Chem. Soc. Dalton Trans. (1992) 2013.
[20] N. Raos, Croat. Chem. Acta 69 (1996) 1189.
[21] J.J. Gajewski, K.E. Gilbert, T.W. Kreek, J. Comp. Chem. 19 (1998) 1167.
[22] I.W. Davies, R.J. Deeth, R.D. Larsen, P.J. Reider, Tetrahedron Lett. 40 (1999) 1233.
[23] P. Comba, T.W. Hambley, M.A. Hitchman, H. Stratemeier, Inorg. Chem. 34 (1995) 3903.
[24] P. Comba, M. Zimmer, Inorg. Chem. 33 (1994) 5368.
[25] P. Comba, T.W. Hambley, M. Strohle, Helv. Chim. Acta 78 (1995) 2042.
[26] R.J. Deeth, M.J. Duer, M. Gerloch, Inorg. Chem. 26 (1987) 2573.
[27] R.J. Deeth, M.J. Duer, M. Gerloch, Inorg. Chem. 26 (1987) 2578.
[28] R.J. Deeth, M. Gerloch, Inorg. Chem. 26 (1987) 2582.
[29] C.R. Landis, T. Cleveland, T.K. Firman, Science 272 (1996) 182.
[30] C.R. Landis, T.K. Firman, D.M. Root, T. Cleveland, J. Am. Chem. Soc. 120 (1998) 1842.
[31] R.J. Deeth, M. Gerloch, Inorg. Chem. 23 (1984) 3846.
[32] R.J. Deeth, Chem. Phys. Lett. 261 (1996) 45.
[33] R.J. Deeth, unpublised results.